

Thermoelastic relaxation near the Curie point of EuO

M. Barmatz and Brage Golding

Bell Laboratories, Murray Hill, New Jersey 07974

(Received 31 October 1973)

An extensive investigation of the acoustic properties of thin EuO reeds has been carried out near the magnetic critical temperature $T_C = 69.3$ K. The main results are the observation of an enhanced damping and velocity dispersion of flexural modes in the frequency range 0.4–3 kHz as $T \rightarrow T_C$. These experimental findings are quantitatively described by Zener's theory of thermoelastic relaxation, taking into account the strong temperature dependences of thermodynamic and transport properties near T_C . The temperature dependences of the adiabatic and isothermal Young's-modulus sound velocities are also obtained. Pippard relations are used to determine the thermodynamic quantities (dP/dT) , (dS/dT) , and (dS/dP) along the transition line.

In this paper we report on an investigation of acoustic properties of EuO near its magnetic critical point. EuO is a face-centered-cubic ferromagnetic insulator with a Curie temperature of 69.3 K. It has been extensively investigated¹ in recent years, since it represents a close approximation to the isotropic Heisenberg ferromagnet. In the present paper we present a complete description of acoustic experiments at low-kilohertz frequencies on thin EuO reeds, in which large sound damping and dispersion are observed near the transition. A preliminary account of this work has been given previously.² We show that this behavior may be accounted for using Zener's thermoelastic relaxation theory.^{3,4} The temperature dependences of the adiabatic and isothermal sound velocities near T_C are determined by correcting the Young's-modulus measurements for thermoelastic dispersion. The thermodynamic quantities (dP/dT) , (dS/dT) , and (dS/dP) along the transition line are determined using generalized Pippard equations which relate the adiabatic and isothermal Young's-modulus velocities to the specific heat at constant pressure near the transition.

Thermoelastic relaxation is an important loss mechanism for thin reeds vibrating in flexure. Zener predicted the existence of this process in 1937³ and the basic aspects of the theory were quickly verified.⁵ Further experimental tests of the theory were provided by Bennewitz and Rötger⁶ on german silver and, more recently, by Berry⁷ on α -brass. In both cases the damping was measured as a function of frequency at room temperature. In the present investigation of EuO, the frequency remained essentially constant and the measurements were carried out as a function of temperature near the magnetic phase transition. This is the first time this process has been studied near a critical point.

I. THEORY

Thermal relaxation may occur whenever a solid experiences a stress inhomogeneity which locally

changes the temperature of the specimen. A sound wave propagating in a solid produces regions of compression and extension which will lead to temperature gradients for materials with a nonzero thermal expansivity. The sound wave loses energy as heat flows from the warmer to cooler regions and this may result in significant sound attenuation. The sound propagation is considered adiabatic if the temperature gradients are not removed by heat flow during half of a sound vibrational period. On the other hand, if the gradients are dissipated within half a sound period, the propagation is isothermal. For example, consider a plane wave traveling in a bulk sample having a positive thermal expansivity, $\beta_p \equiv (1/V)(\partial V/\partial T)_p > 0$. As shown in Fig. 1(a) the compressed regions will be heated while the extended regions are cooled. For a thermal wave $\omega = Dk^2$, where D is the thermal diffusivity and k is the wave vector. Thus the thermal wave velocity is $c = (D\omega)^{1/2}$ and we have adiabatic propagation at low frequencies where $c < v$, v being the sound velocity, which is essentially constant. At high frequencies $c > v$ and isothermal conditions prevail. The condition $c = v$ defines the crossover from adiabatic to isothermal behavior for a plane wave. The crossover frequency is $\omega_c = v^2/D$, shown in Fig. 1(c).

The situation is quite different for a reed of the same material vibrating in flexure. Let us consider a segment of such a reed of thickness d , shown in Fig. 1(b). The layers below the neutral plane (dashed line) are compressed during this part of the vibration cycle and are heated, while the layers above the neutral plane are extended and cooled. Again heat flows from the warmer to cooler layers. Now, however, the temperature gradient always extends over the sample thickness regardless of frequency. Thus at low frequencies, there is sufficient time for the thermal gradient to be removed, since the sound period is very long. This leads to isothermal propagation. For higher frequencies the sound period becomes so short that

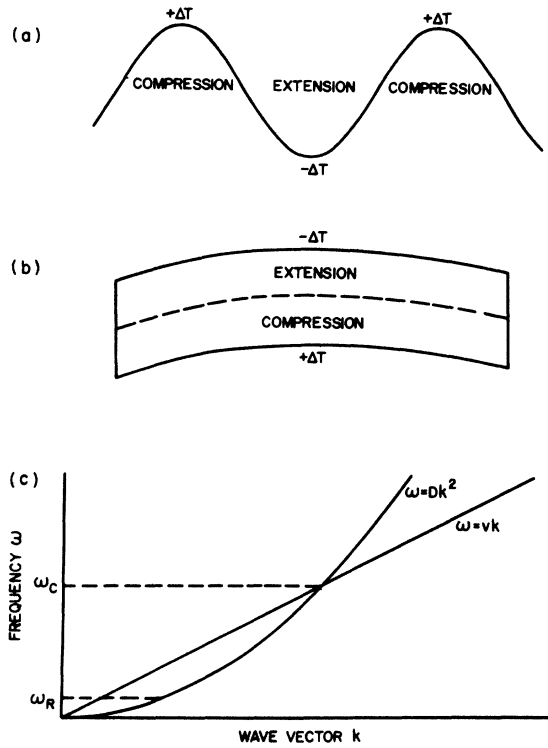


FIG. 1. Adiabatic and isothermal sound propagation: (a) regions of extension and compression for plane-wave propagation, (b) segment of a reed vibrating in flexure, (c) dispersion curves for sound and thermal propagation. The frequencies ω_R and ω_C represent crossover frequencies for flexural and plane-wave propagation, respectively.

the heat does not have time to traverse the reed thickness and adiabatic conditions exist. The crossover occurs when heat crosses the sample in approximately half a sound period. The corresponding frequency is $\omega_R \approx (\pi/d)^2 D$, which is also shown in Fig. 1(c). In most dielectrics ω_C corresponds to frequencies higher than the GHz range while ω_R may be adjusted to lie in the audio range 10^2 – 10^4 Hz. The vibrating-reed technique is thus a good method for exploring the thermal behavior of solids at low frequencies. The EuO measurements presented here cover both the adiabatic and isothermal regimes of the reed.

The Zener theory of damping by transverse thermal modes in reeds showed that the relaxation behavior may be represented by a discrete spectrum of relaxation times which led to a total relaxation rate Γ ,

$$\Gamma = \omega Q^{-1} = A(T) \sum_{j=0}^{\infty} f_j \frac{\omega^2 \tau_j}{1 + \omega^2 \tau_j^2}, \quad (1)$$

where the relaxation strength $A(T) = TE_T \alpha_p^2 / C_p$, and E_T , α_p , and C_p are the isothermal Young's

modulus, linear thermal expansivity, and isobaric specific heat, respectively. f_j and τ_j are the relative strength and characteristic relaxation time for the j th-order process. The expression for Γ given by this equation is valid so long as the relaxation strength $A(T) \lesssim 10^{-2}$. For a thin rectangular reed the strain is a function only of the transverse distance from the neutral plane and the calculation of the relative strengths and relaxation times gives

$$f_j = (96/\pi^4)(2j+1)^{-4} \quad (2)$$

and

$$\tau_j^{-1} = [(2j+1)(\pi/d)]^2 D, \quad (3)$$

where $D = \lambda/C_p$ is the thermal diffusivity, with λ the total thermal conductivity. Evaluating the first few weighting factors from Eq. (2), $f_0 = 0.968$, $f_1 = 0.012$, and $f_2 = 0.0016$, shows this series is strongly convergent and little error ($\lesssim 2\%$) is made by retaining only the first term. For the analysis of the EuO measurements we assume the damping constant Γ and the Young's-modulus dispersion satisfy the single relaxation expressions

$$\Gamma(\omega, T) = A(T) \omega \Re(\omega\tau) \quad (4)$$

and

$$[E(\omega, T) - E_T(T)]/E_T(T) = A(T) \omega \tau \Re(\omega T), \quad (5)$$

where $E_T(T)$ is the isothermal Young's modulus.⁸ The relaxation function $\Re(\omega\tau)$ is defined⁸ by

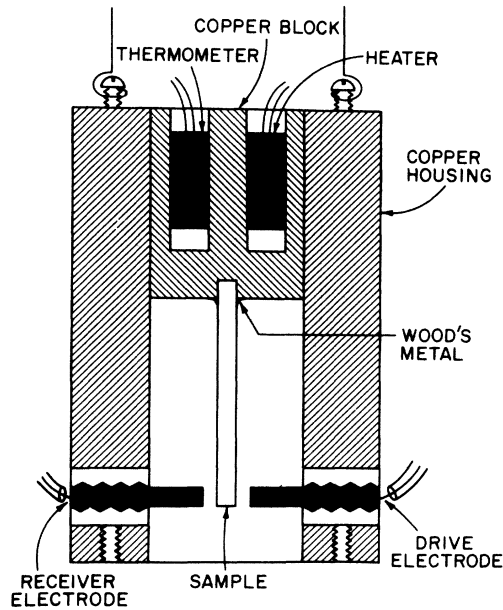


FIG. 2. Sample holder. The Au-sputtered EuO sample was soldered to a copper block containing the thermometer and heater used to measure and control the sample temperature. The sample holder was suspended from an evacuated inner can by stainless-steel wires.

$$\Re(\omega\tau) \equiv \omega\tau / (1 + \omega^2\tau^2), \quad (6)$$

with

$$\tau(T) = (d/\pi)^2 D^{-1}(T). \quad (7)$$

In materials exhibiting phase transitions, the thermoelastic process may be considerably enhanced near the transition temperature. As T approaches T_C , the quantities C_p and α_p become singular and thus the relaxation strength and relaxation time will increase over a small temperature region near T_C . In recent years thermodynamic properties near critical points have been measured with high precision. This information coupled with acoustic measurements may be used to critically test the predictions of the thermoelastic relaxation process.

II. TECHNIQUE

The Young's modulus and damping constant were measured using a vibrating-reed technique. The samples were EuO single crystals of width 0.4 cm and length 1.0 cm, with the long axis along $\langle 110 \rangle$. At 300 K, the measured resistivity of the EuO was $\rho \approx 10^7 \Omega \text{ cm}$. We investigated two samples, one (designated I) with a thickness $d = 0.016 \text{ cm}$ and a second thinner sample (II) with $d = 0.0065 \text{ cm}$. A gold film ($\sim 2000 \text{ \AA}$) was sputtered on all sample surfaces to make them conducting. Sample I was resonated at its fundamental frequency of 1600 Hz and gave the most accurate data. The thin sample (II) was primarily used to confirm that τ varied as d^2 . Simultaneous measurements at its fundamental (433 Hz) and second overtone (2785 Hz) also yielded dispersion information. A schematic of the sample holder is shown in Fig. 2. One end of the sam-

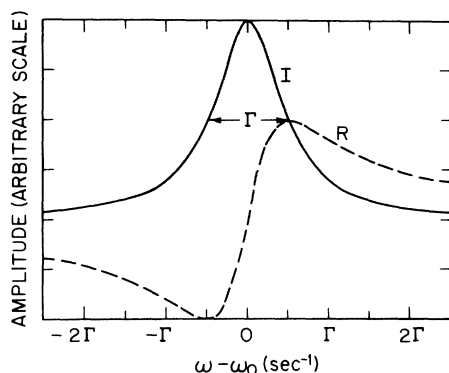


FIG. 3. The real and imaginary components of a single mechanical resonance. ω_0 and Γ denote the resonant frequency and decay rate, respectively. The real component (dashed line) is an antisymmetric function of $\omega - \omega_0$ and reaches its extrema at the half-power points of the resonance given by $\omega_- = \omega_0 - \frac{1}{2}\Gamma$ and $\omega_+ = \omega_0 + \frac{1}{2}\Gamma$. The width at half-maximum for the imaginary component (solid line) is the decay rate Γ .

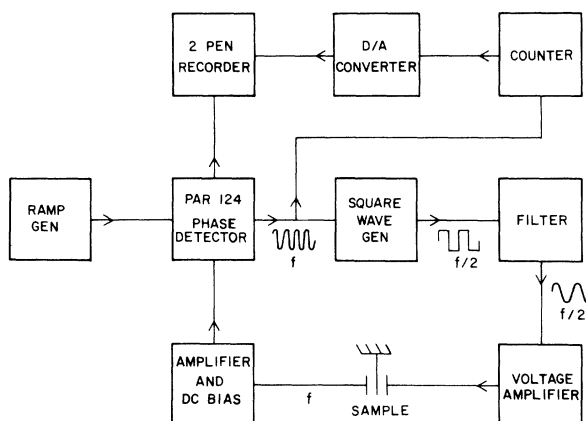


FIG. 4. Electronic system I. This system measured the fundamental flexural resonances of samples I and II. The PAR-124 oscillator was voltage controlled by a ramp generator and the real or imaginary component of the sample resonance was recorded as the frequency was swept through the resonance. Sweep rates ranged from 0.1–0.6 Hz/min.

ple was soldered with Wood's metal to a copper block. A copper housing, which contained the drive and pickup electrodes, clamped the copper block so that the free end of the sample was situated between the two electrodes. The gap between the sample and electrodes was typically 0.015 cm. Two stainless-steel wires isolated and supported the copper housing from an inner evacuated can. The inner can's temperature could be controlled with a heater and thermometer mounted on it. The inner can was further thermally isolated by supporting it inside a large outer can which could also be evacuated. The pressure in the double-can system was reduced to 10^{-4} Torr during measurements. A 100- Ω carbon resistor heater and a 1000- Ω platinum thermometer were situated in the copper block holding the sample. The sample temperature was measured with the Pt thermometer using a standard ac resistance bridge with phase-sensitive detection. The sample temperature was controlled to better than $\pm 2 \times 10^{-3}$ K by using the bridge off-balance signal to regulate the heater current.

For a clamped reed of rectangular cross section, the flexural resonant frequencies⁹ are

$$f_n = (\mathcal{K}/2\pi)(k_n/l)^2 v, \quad (8)$$

where $\mathcal{K} = d/(12)^{1/2}$ is the radius of gyration, l is the length of the reed, and the k_n 's are constants 1.875, 4.694, 7.855, ... for $n=1, 2, 3, \dots$. The quantity $v = (E/\rho)^{1/2}$ is the Young's-modulus velocity along the reed, with E being the Young's modulus and ρ the density. Thus, the Young's-modulus velocity along the reed is directly propor-

tional to the flexural resonant frequency. Equation (8) is valid for $\lambda_n \gg \mathcal{X}$, where λ_n is the flexural wavelength of the n th mode ($\lambda_n = 2\pi l/k_n$). This condition is satisfied for all frequencies measured in this investigation.

The acoustic properties at resonance were determined using a vector-component technique. Let us consider the motion of a damped mechanical oscillator excited by a complex driving force $F_0 e^{i\omega t}$. The equation of motion for the displacement of this system is

$$m\ddot{x} + R_m \dot{x} + sx = F_0 e^{i\omega t}, \quad (9)$$

where m , R_m , and s are the mass, mechanical resistance, and stiffness constant, respectively. The steady-state solution of Eq. (9), assuming the displacement has the form $x = x_0 e^{i\omega t}$, is

$$x_0 = \frac{F_0/m}{(\omega_0^2 - \omega^2) + i\omega\Gamma}, \quad (10)$$

where $\omega_0 = (s/m)^{1/2}$ and $\Gamma = R_m/m$ are the resonant frequency and damping constant, respectively. Under the condition that the quality factor of the system $Q \equiv \omega_0/\Gamma \gg 1$, which is the case in this investigation, the real (R) and the imaginary (I) components of the displacement amplitude have the form

$$R = \frac{(\omega_0^2 - \omega^2)(F_0/m)}{(\omega_0^2 - \omega^2)^2 + \omega_0^2 \Gamma^2}, \quad (11)$$

$$I = \frac{-\omega_0 \Gamma (F_0/m)}{(\omega_0^2 - \omega^2)^2 + \omega_0^2 \Gamma^2}. \quad (12)$$

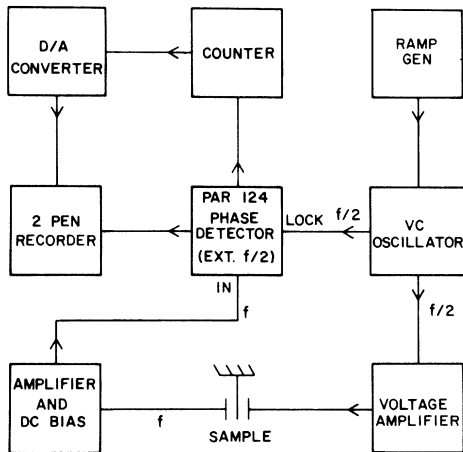


FIG. 5. Electronic system II. This system measured the second overtone of sample II. The PAR-124 detector was phase-locked to an external oscillator which was voltage controlled. As with electronic system I, the frequency was swept through the flexural resonance and the frequency and resonant shape were recorded as a function of time. For the 433-Hz resonance, sweep rates were typically 0.02 Hz/min.

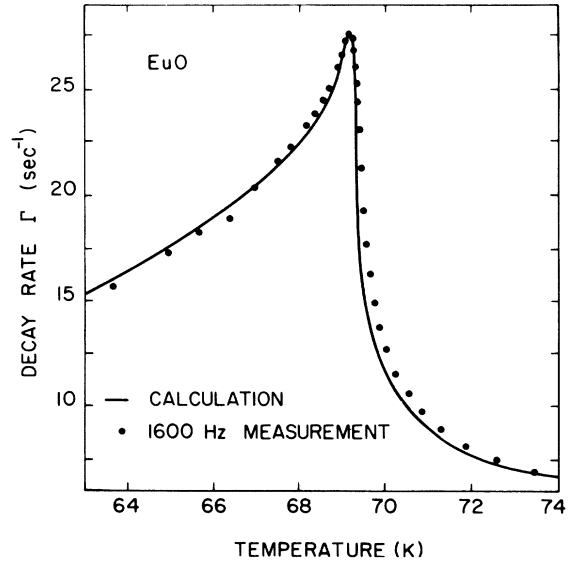


FIG. 6. Temperature dependence of the decay rate Γ for 1600 Hz flexural vibrations. The solid curve is the calculated damping from the thermoelastic relaxation process. No adjustable parameters, scale factors, or background terms were used in this comparison of absolute decay rates.

These resonant components are shown as a function of frequency in Fig. 3. All pertinent information concerning the resonance can be obtained from either component. However, in the present investigation we chose to concentrate on the real part. The component R is an antisymmetric function of ω with respect to ω_0 , and its maximum and minimum occur at the half-power frequencies $\omega_- = \omega_0 - (\Gamma/2)$ and $\omega_+ = \omega_0 + (\Gamma/2)$. The resonant frequency and damping constant can thus be obtained from a plot of this component versus frequency. A fit of Eq. (11) to the data utilizing a four-parameter nonlinear-least-squares routine was used to determine the parameters ω_0 and Γ for each temperature. The standard deviations for ω_0 and Γ from the computer fit were typically $2 \times 10^{-4}\%$, and 0.4%, respectively.

The measurements of the sound damping and dispersion were carried out with either of two electronic systems, each using phase sensitive detection. For the thin sample (II), we investigated both the first and second overtones. In this case it was advantageous to use both electronic systems simultaneously to obtain data for the two modes under the same experimental conditions. Figure 4 shows the electronics associated with the first-measurement technique. The phase-detector's internal oscillator was voltage controlled by a ramp generator and produced a cw sine wave of frequency f . This signal was converted to a square

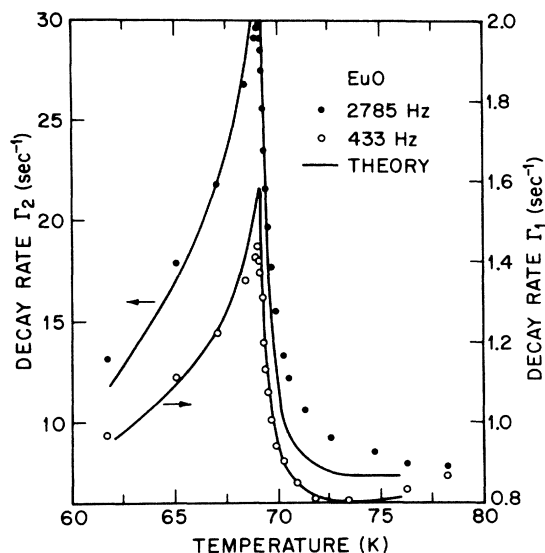


FIG. 7. Decay rate vs temperature for the two overtones of sample II. The solid curves are the predictions of the thermoelastic theory. A constant background loss of 0.65 sec^{-1} is included in the 433 Hz theoretical curve (right-hand ordinate).

wave whose period was twice that of the input signal. A filter tuned to the fundamental of the square wave yielded a sine wave of frequency $f/2$, which was applied to the drive transducer after appropriate amplification. Drive signals were typically 25 V. The unbiased-drive transducer drove the sample at twice the applied frequency. The receiver transducer was biased with 200-V dc and detected the flexural vibrations at frequency f through the resultant variation in the receiver capacitance. After amplification, the received signal was fed to the phase detector. Received signals at the phase detector were typically 10–20 mV. The unbiased-drive-biased-receiver arrangement used here has the attractive feature that any pick-up of the drive signal is at half the frequency of interest and can be filtered out in the receiver. By adjusting the phase of the received signal relative to the internal oscillator, the real or imaginary component of the resonance could be selected. The phase-detector dc output and the resonant frequency were recorded as the frequency was swept through the flexural resonance. Twelve to 20 min were necessary to record a resonance curve using sweep rates as low as 0.01 Hz/min. The second electronic system employed is shown in Fig. 5. In this case an external oscillator at $f/2$ is voltage controlled by the ramp generator. The phase-detector oscillator is then phase-locked to twice the frequency of the external oscillator. The rest of the circuit is similar to that of the first-measure-

ment technique discussed above. With a slight modification, the two electronic systems could also track continuously the resonant frequency as a function of temperature. This was accomplished by replacing the ramp-generator signal with the dc output from the phase detector.

III. RESULTS

A. Damping

The measured decay rate Γ for the thick reed (sample I) is shown in Fig. 6 for the temperature range $T_C \pm 5 \text{ K}$. The data are for the fundamental frequency of 1.6 kHz and were obtained under thermal equilibrium conditions. A test of the thickness dependence of the thermoelastic relaxation time given in Eq. (7) was made using sample II, which was a factor of 2.2 thinner than sample I. For this thin sample, simultaneous measurements were carried out at two resonant frequencies using the electronic apparatus shown in Figs. 4 and 5. The results for the sound damping at the two lowest overtones are shown in Fig. 7.

B. Dispersion

The simultaneous measurement of the fundamental and second overtone of sample II permitted the determination of sound dispersion between the two frequencies. Because of experimental difficulties we took data only above the transition, as is shown in Fig. 8. We observed a rather small time-dependent background change $\Delta v/v \approx 7 \times 10^{-5}/\text{day}$ in the fundamental resonance. This behavior was probably due to long equilibration times associated

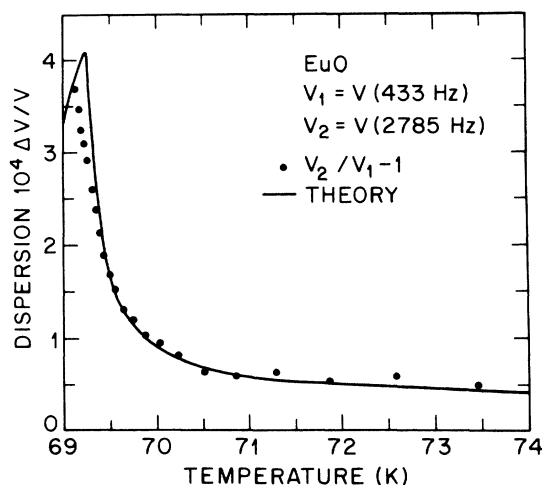


FIG. 8. Temperature dependence of thermoelastic dispersion. The experimental dispersion was obtained from the ratio of resonant frequencies. The solid curve is the theoretical expectation for the two lowest overtones of sample II.

with stress release accompanying temperature change in the Wood's metal-copper bond. The dispersion measurements were taken over several days and the data were corrected for background drift.

C. Velocity

The temperature dependence of the $[110]$ Young's-modulus velocity near the EuO Curie point is shown in Fig. 9 for the fundamental of sample I. These data also represent measurements taken over a period of several days. This was necessary because of the wide temperature range covered (~ 10 K) and the fact that measurements were taken only after equilibrium conditions were attained. For large temperature changes, the equilibration time was ~ 1 h.

IV. DISCUSSION

A. Thermoelastic properties

The temperature dependences of the thermodynamic and transport properties needed to compute the relaxation strength A and the time constant τ were measured on samples cut from the same single-crystal boule used in the present investigation. Variations in the measurements due to dif-

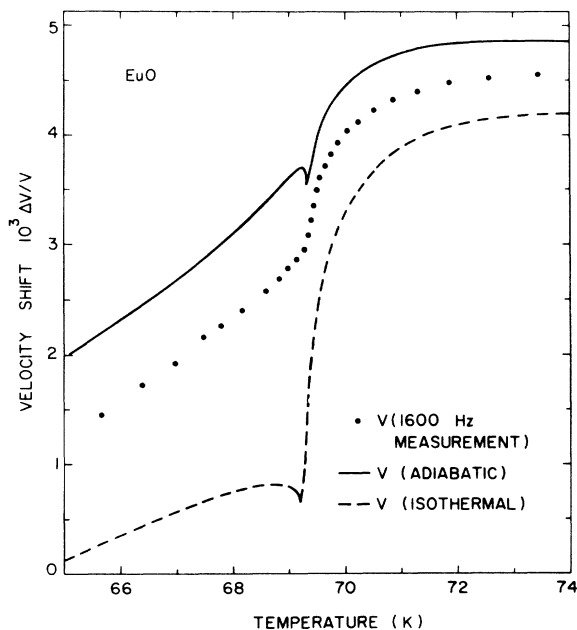


FIG. 9. Temperature dependence of the $\langle 110 \rangle$ Young's-modulus velocity for 1.6-kHz flexural vibrations in EuO near T_C . The solid and dashed lines are the adiabatic and isothermal velocities, respectively, calculated from thermoelastic relaxation theory and the experimental data.

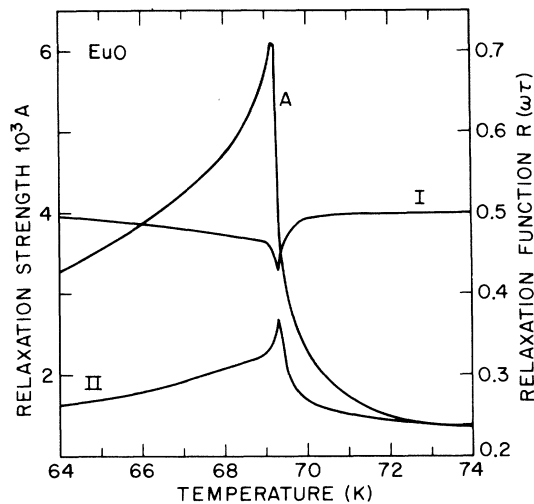


FIG. 10. Temperature dependence of the thermoelastic relaxation strength $A(T)$ and the relaxation function $\mathcal{R}(\omega\tau)$. Curves I and II correspond to $\mathcal{R}(\omega\tau)$ for samples I and II, respectively. The temperature variation between curves I and II near T_C arises from the fact that for sample I $\omega\tau \gtrsim 1$, while for sample II, $\omega\tau < 1$.

ferences in sample preparation were thus minimized. The thermal expansivity was measured in the temperature range 62–76 K by a capacitance technique described previously.¹⁰ Specific-heat data were obtained from the recent measurements of Kornblit, Ahlers, and Buehler.¹¹ An ac technique was used to measure the thermal diffusivity¹² of a thin EuO reed, similar in size to the acoustic samples. We have used the data for α_p , C_p , and E to calculate the expected relaxation strength for the thermoelastic process which is shown in Fig. 10. Also shown is the relaxation function $\mathcal{R}(\omega\tau)$ for samples I and II. The temperature dependence of the damping constant Γ comes primarily from the relaxation strength rather than $\omega\tau$. As the transition is approached from above the relaxation strength increases by a factor of 5 and reaches a sharp maximum near T_C . The rounding of the relaxation strength near the transition is probably due to the effects of sample inhomogeneity. Near T_C the relaxation function $\mathcal{R}(\omega\tau)$ exhibits different temperature dependent behavior for the two samples, since $\omega\tau \gtrsim 1$ for sample I while $\omega\tau < 1$ for sample II.

The decay rate expected from the thermoelastic process is obtained from the relaxation strength A and the relaxation function $\mathcal{R}(\omega\tau)$, using Eq. (4). The solid curve in Fig. 6 represents the prediction of the thermoelastic theory for sample I. No adjustable parameters, scale factors, or background terms were employed in this comparison of absolute decay rates. Other possible contributions to the

measured decay rate near the transition may arise from critical relaxation processes and domain losses (below T_c). However, it can be shown that these processes lead to a negligible contribution to the decay rate at these frequencies.^{13,14} The excellent agreement between the theory and experiment is remarkable, taking into account possible uncertainties in the absolute values and temperature variations in the separate experiments for α , C_p , and D . These damping measurements confirm the predictions of Zener's thermoelastic theory to better than a few percent.

Sound damping observed in the thin sample (II) was also compared to the thermoelastic theory. In Fig. 7 the solid lines again represent the theoretical prediction for the measured frequencies. In the case of the fundamental frequency of 433 Hz the total damping is so small that the contribution from background terms, probably due to clamping, becomes significant. To account for this clamping loss, a constant background damping term of 0.65 sec⁻¹ has been included in the theoretical curve for this frequency. There is good agreement between the low-frequency measurements and theory, except very near T_c . The high-frequency data, on the other hand, are only represented reasonably well by thermoelastic loss. However, the fit could be improved by including an arbitrary constant background term, as was done for the lower frequency. Both sets of data from sample II show an excessive amount of rounding near T_c as compared to sample I. We attribute this enhanced rounding to strains introduced in the sample by lapping. The thermoelastic dispersion between the two resonances of sample II is represented by the solid curve in Fig. 8 and is seen to agree well with the measurements above 69.5 K. Closer to the transition, there is a rounding in the data similar to that observed for Γ_1 and Γ_2 in Fig. 7.

Near a second-order phase transition the sound velocity experiences a dip as the critical temperature is approached from either above or below. The magnitude of the velocity dip depends on the coupling between the velocity and other singular thermodynamic parameters. The EuO measurements in Fig. 9 show the expected sharp drop in velocity as the transition is approached from above. However, below T_c the sound velocity does not immediately rise. Instead, there is an inflection point at the transition and the velocity continues to decrease for approximately 20 K before it again has a negative temperature coefficient. The velocity behavior below the transition may be accounted for by two effects, (a) magnetic domain interactions, which cause a reduction in the sound velocity, and (b) dispersion associated with the thermoelastic relaxation. The effects of domains on the velocity below T_c cannot be interpreted at

this time owing to lack of information on domain properties in EuO. The good agreement between the thermoelastic theory and sound damping shown in Fig. 6 gives us confidence in using the theory to correct the measurements for dispersion. We used Eq. (5) and the data to compute the temperature dependence of the adiabatic and isothermal velocities shifts as shown in Fig. 9 by the solid and dashed curves, respectively. The removal of dispersion effects reveals a small minimum in $\Delta v/v$ in both the adiabatic and isothermal cases.

The velocity data corrected for dispersion may be used to estimate the relaxation strength for the critical relaxation process. At 1.6 kHz, we are essentially measuring the "zero" frequency or adiabatic velocity, $v_c(0)$, for this process, which is given by the adiabatic curve in Fig. 9. The infinite-frequency velocity, $v_c(\infty)$, for the critical process is identified with the unperturbed lattice or background velocity. $v_c(\infty)$ is estimated by extrapolating the adiabatic velocity well above the transition to T_c . This leads to a critical relaxation strength

$$[v_c^2(\infty) - v_c^2(0)]/v_c^2(0) \approx 2 \times 10^{-3} .$$

A knowledge of the critical relaxation strength is important in interpreting recent ultrasonic measurements¹³ at 230 kHz which explore the critical relaxation process.

B. Thermodynamic properties

Various relations among thermodynamic quantities have been proposed near a λ transition. Pippard's original derivation¹⁵ related the specific heat at constant pressure C_p , the isobaric thermal expansion coefficient β_p , and the isothermal compressibility \mathcal{K}_T by the expressions

$$C_p/T = \xi V \beta_p + \text{const} , \quad (13)$$

$$\beta_p = \xi \mathcal{K}_T + \text{const} , \quad (14)$$

where $\xi = (dP/dT)_\lambda$ is the slope of the λ line and V is the specific volume. These relations, which give the asymptotic behavior as the transition is approached, have been successfully used to determine thermodynamic properties along λ lines.¹⁶ The Pippard equations were generalized by Garland¹⁷ to stress-strain variables and by Janovec¹⁸ for transitions in anisotropic dielectrics. From the expression for the Gibbs free energy in terms of stresses and temperature near a λ point, Garland derived the following relations:

$$\alpha_i = \xi_i^{-1} (C_p/V T) - g'_i , \quad (15)$$

$$S_{ij}^T = \xi_j^{-1} \alpha_i - \xi_i^{-1} g'_j - t g''_{ij} \delta_{ij} - h^{(ij)} , \quad (16)$$

where S_{ij}^T are the isothermal elastic compliances. The quantities α_i and $\xi_i^{-1} = (\partial T_\lambda / \partial X_i) X_{j \neq i}$ are the linear expansion coefficient and slope of the λ line,

respectively, along the i th axis. The primes denote differentiation of the slowly varying function g with respect to the i th or j th axial stress component. The symbol δ_{ij} is Kronecker's delta, $t = T - T_\lambda(X_j)$ where X_j is the stress component along the j th axis, and the superscript on the slowly varying function h denotes differentiation with respect to the i th and j th component. Garland also showed that the adiabatic elastic compliances S_{ij}^s are given by

$$S_{ij}^s = \text{const} - g'_i g'_j (VT/C_p). \quad (17)$$

For a cubic system $\xi_i^{-1} = \xi_j^{-1} = \frac{1}{3} (dT/dP)_\lambda$ and $g'_i = g'_j = (1/3V) (dS/dP)_\lambda$.

In this experiment, we have corrected the modulus data to obtain the isothermal and adiabatic Young's modulus along the $\langle 110 \rangle$ direction. For a cubic system such as EuO, the $\langle 110 \rangle$ isothermal modulus is related to the isothermal compliances by

$$(E_{110}^T)^{-1} = \frac{1}{2}(S_{11}^T + S_{12}^T) + \frac{1}{4}S_{44}^T. \quad (18)$$

This expression is also valid for the $\langle 110 \rangle$ adiabatic modulus E_{110}^S if the compliances are replaced by their adiabatic counterparts.

Eliminating α_i from Eq. (16) and substituting the appropriate compliances in Eq. (18) yields a simple expression relating the isothermal $\langle 110 \rangle$ velocity $v_T = (VE_{110}^T)^{1/2}$ to the specific heat in a cubic system, i. e.,

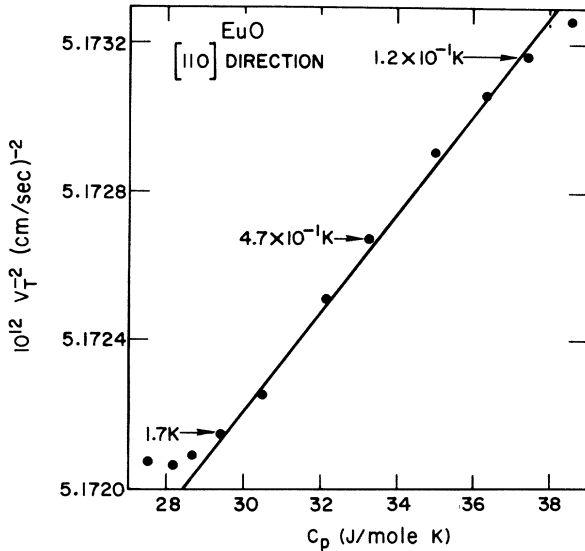


FIG. 11. The inverse square of the $[110]$ isothermal velocity v_T vs the specific heat C_p . The arrows indicate the temperature difference $T - T_C$. The generalized Pippard relations predict a linear relationship, Eq. (19), between v_T and C_p in the asymptotic limit as $T \rightarrow T_C$. The solid line corresponds to $(dT/dP)_\lambda = 0.45$ K/kbar.

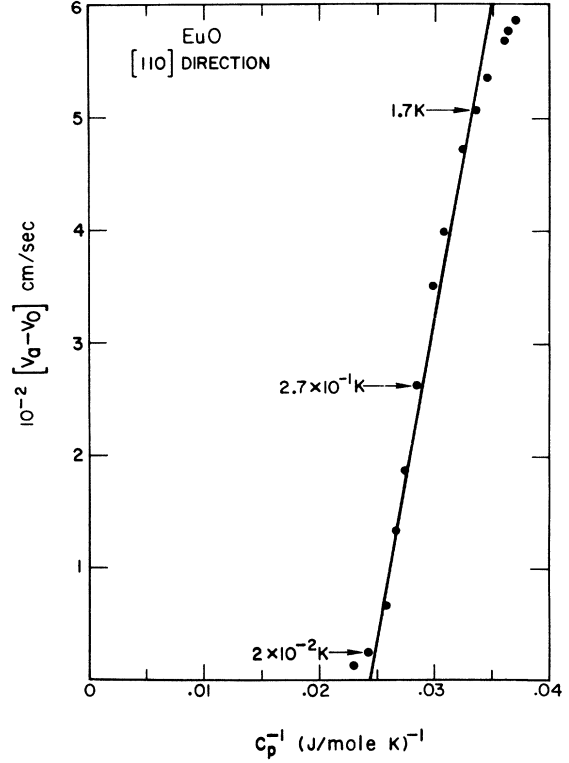


FIG. 12. A Pippard plot of the $[110]$ adiabatic velocity difference $v_a - v_0$ vs the reciprocal specific heat, C_p^{-1} . The arrows indicate the temperature difference $T - T_C$. The minimum velocity measured experimentally, v_0 , is 4.176×10^5 cm/sec. The solid line gives $(dS/dP)_\lambda = 1.3 \times 10^{-5}$ cm³/gK.

$$v_T^{-2}(T) = A_1 C_p(T) + B_1, \quad (19)$$

where A_1 and B_1 are constants (within the asymptotic approximation) with $A_1 = (9V^2 T_\lambda)^{-1} (dT/dP)_\lambda^2$. In this derivation we have assumed that S_{44}^T is a regular function of t . A similar derivation for the adiabatic modulus using Eq. (18) yields

$$[E_{110}^s(T)]^{-1} = A_2 C_p^{-1}(T) + B_2, \quad (20)$$

where again A_2 and B_2 are constants. The C_p term in this equation will vanish at the transition for a diverging specific heat and will give $[E_{110}^s(T_\lambda)]^{-1} = B_2$. In the case of EuO, however, the measured C_p may be nondivergent and thus would be finite at $T_\lambda (= T_C$ for the EuO case). Thus, in general, the expected modulus at the transition is given by Eq. (20) for $T = T_\lambda$. Equation (20) may be simplified by introducing the adiabatic Young's-modulus velocity v_a and expanding $v_a^{-2}(T)$ about its value $v_a^{-2}(T_\lambda)$ at the transition. By referring the velocity to the minimum value measured experimentally, v_0 , we finally obtain

$$v_a(T) - v_0 = A[C_p^{-1}(T) - C_p^{-1}(T_\lambda)] + B, \quad (21)$$

where $A = [T_\lambda v_a^3(T_\lambda)/18V^2] (dS/dP)_\lambda^2$ and $B = v_a(T_\lambda) - v_0$. We see that a comparison of the isothermal and adiabatic EuO velocities with the specific heat will yield the thermodynamic quantities dT/dP and dS/dP along the transition line.

The experimental resonant frequency data were normalized to the measurements of Shapira and Reed¹⁹ at 78 K to obtain the absolute velocity. In Fig. 11 the inverse square of the isothermal velocity measured above the transition is plotted against C_p using the specific-heat values of Kornblit *et al.*¹¹ given by

$$C_p = \left(\frac{A'}{\alpha}\right) \left(\left|\frac{T - T_c}{T_c}\right|^{-\alpha} - 1\right) + B' + \frac{D(T - T_c)}{T_c}, \quad (22)$$

where $\alpha = -0.0418$, $A' = 4.189$, $B' = 14.14$, and $D = 33.55$ for C_p in J/mole K. The straight line drawn through the data yields $(dT/dP)_\lambda = 0.45$ K/kbar for the slope of the transition line [see Eq. (19)]. This value, which is larger than 0.34 K/kbar quoted by Argyle *et al.*²⁰ is in good agreement with the value 0.47 K/kbar determined from a plot [Eq. (13)] of C_p vs β_p for EuO.²¹ Since C_p is assumed finite at the transition, the isothermal velocity does not vanish at T_λ , but will reach the minimum value of 4.13×10^5 cm/sec which is $\sim 1\%$ less than v_0 .

We show the adiabatic velocity as a function of C_p^{-1} in Fig. 12. The data are consistent with the expected linear relationship, Eq. (21), over the temperature range $0.02 < T - T_\lambda < 1.7$ K. The isothermal velocity satisfied Eq. (19) over approximately the same temperature interval. Deviations from linear behavior very near T_λ are probably due to inhomogeneity effects. The straight line in Fig. 12 gives $(dS/dP)_\lambda = 1.3 \times 10^{-5}$ cm³/gK and $v_a(\lambda) = 4.167 \times 10^5$ cm/sec. The expected velocity at the transition is $\sim 0.22\%$ below v_0 . By using the

values of $(dS/dP)_\lambda$ and $(dT/dP)_\lambda$ determined in this experiment, we find $(dS/dT)_\lambda = 2.9 \times 10^4$ erg/gK². This may be compared to $(dS/dT)_\lambda = 1.3 \times 10^4$ erg/g K² obtained from Eq. (13).²¹

V. CONCLUSION

We have shown that flexural damping and dispersion near the EuO magnetic phase transition may be quantitatively accounted for by the thermoelastic relaxation theory. In the case of the thermoelastic process, the enhancement of these acoustic properties near T_c is primarily due to an increase in the relaxation strength rather than in $\omega\tau$. This is in contrast to most other critical processes where it is tacitly assumed that the $\omega\tau$ dependence controls the relaxation process. The thermoelastic theory contains no adjustable parameters and thus it may be useful in determining critical properties in solids. For example, in cases where sufficient thermodynamic data exist, it should be possible to measure the thermal diffusivity using thermoelastic relaxation.

We have used the vibrating-reed technique to investigate both the adiabatic and isothermal velocity regimes near T_c in EuO. The temperature dependence of the adiabatic and isothermal velocities in conjunction with generalized Pippard relations have yielded the thermodynamic quantities $(dT/dP)_\lambda$, $(dS/dP)_\lambda$, and $(dS/dT)_\lambda$, which are consistent with other available measurements.

ACKNOWLEDGMENTS

We thank M. B. Salamon for providing us with EuO diffusivity data prior to publication and to E. Buehler for growing the excellent EuO sample. The valuable comments of P. C. Hohenberg and the technical assistance of V. Chirba are also acknowledged.

¹See L. Passell, O. W. Dietrich, and J. Als-Nielsen, AIP Conf. Proc. No. 5, 1251 (1971) and references therein.

²Brago Golding, M. Barmatz, E. Buehler, and M. B. Salamon, Phys. Rev. Lett. **30**, 968 (1973).

³C. Zener, Phys. Rev. **52**, 230 (1937); Phys. Rev. **53**, 90 (1938).

⁴C. Zener, *Elasticity and Anelasticity of Metals* (University of Chicago Press, Chicago, 1948), p. 89.

⁵C. Zener, W. Otis, and R. Nuckolls, Phys. Rev. **53**, 100 (1938).

⁶K. Bennewitz and H. Rötger, Z. Tech. Phys. **XIX**, 521 (1938).

⁷B. S. Berry, J. Appl. Phys. **26**, 1221 (1955).

⁸It should be noted that in Eq. (2) of Ref. 2, E_T was erroneously replaced by E_S . Also the relaxation function $\mathcal{R}(\omega\tau)$ defined here has a different form than $\mathcal{R}(\omega, \tau)$ used in Ref. 2.

⁹S. Timoshenko, in *Vibration Problems in Engineering*, 3rd ed. (Van Nostrand, Princeton, N. J. 1955), p. 338.

¹⁰B. Golding, Phys. Rev. Lett. **27**, 1142 (1971); and J.

Appl. Phys. **42**, 1381 (1971).

¹¹A. Kornblit, G. Ahlers, and E. Buehler, Phys. Lett. **43A**, 531 (1973).

¹²P. R. Garnier, M. B. Salamon, B. Golding and E. Buehler (unpublished).

¹³We have recently investigated (see Ref. 2) critical relaxation in EuO using a resonant-bar technique at 230 kHz. The measurements indicate that the critical relaxation rate $\tau_c^{-1} \approx 1.5 \times 10^6$ sec⁻¹. Combining this rate with the critical relaxation strength of 2×10^{-3} leads to a decay rate of $\Gamma_c \approx 0.13$ sec⁻¹ at 1.6 kHz (unpublished).

¹⁴We have observed attenuation maxima due to domain losses in EuO at temperatures 0.9 and 25 K below T_c at frequencies of 230 kHz and 20 MHz respectively. Using these data and the corresponding maximum decay rates, we have extrapolated the expected domain loss to 1.6 kHz. This leads to a maximum decay rate $\Gamma_m \approx 2$ sec⁻¹ at $T_c - T \approx 2 \times 10^{-2}$ K. This maximum is so close to T_c that we would expect it to be smeared out due to rounding effects.

¹⁵A. B. Pippard, Philos. Mag. **1**, 473 (1956).

¹⁶See for example, M. Barmatz and I. Rudnick, Phys. Rev. 170, 224 (1968).

¹⁷C. W. Garland, J. Chem. Phys. 41, 1005 (1964).

¹⁸V. Janovec, J. Chem. Phys. 45, 1874 (1966).

¹⁹Y. Shapira and T. B. Reed, J. Appl. Phys. 40, 1197

(1969).

²⁰B. E. Argyle, N. Miyata, and T. D. Schultz, Phys. Rev. 160, 413 (1967).

²¹B. Golding, Bull. Am. Phys. Soc. 19, 271 (1974).